Supplementary information

Experimental Section

Preparation of electrolytes

A baseline electrolyte of 2 M $ZnSO_4$ was prepared by dissolving Zinc sulfate ($ZnSO_4 \cdot 7H_2O$, AR) in deionized water. D- pantothenic acid (0, 5, 10, 15, 20, 25v/v%) was added to the prepared 2 M $ZnSO_4$ electrolyte to obtain $ZnSO_4$+D-PA electrolyte.

Synthesis of cathode

$NH_4V_4O_{10}$ (NVO) powder was prepared according to the previous references. 0.9359 g NH_4VO_3 (8 mmol) was dissolved in 60 mL deionized water at 60 °C and cooled to room temperature, and 1.0085 g oxalic acid (8 mmol) was taken separately and dissolved in 10 mL deionized water. Then the prepared oxalic acid aqueous solution was added slowly dropwise to NH_4VO_3 aqueous solution and stirred vigorously for 30 min. The mixed solution was transferred to 100 mL Teflon-lined autoclave and heating at 180 °C for 24 h. After cooling, the product was collected and washed repeatedly with deionized water and ethanol, respectively, and finally dried at 60 °C for 12 h to obtain the NVO material. NVO, super P, and PVDF at a ratio of 7:2:1 was mixed in N-methyl pyrrolidone (NMP). The prepared slurry was coated on 14 mm C paper at a mass loading of 2~3 mg cm^{-2}. Then the slices dried in a vacuum oven at 60 °C for 12 h to finish the production of NVO cathode.

Materials characterizations

The surface morphology images of samples were observed by scanning electro microscopy (SEM, JSM-7500F). The texture analysis was performed via the X-ray diffraction (XRD, Bruker). The surface composition of samples was obtained with the X-ray photoelectron

spectroscopy (XPS, Thermo Scientific K-Alpha). The characterization of electrolyte properties by Fourier-transform infrared spectroscopy (FTIR, Thermo Fisher Scientific Nicolet iS20), nuclear magnetic resonance (NMR, Bruker Plus 400MHz), and Raman spectroscopy (Raman, HORIBA HR Evolution). The dendritic growth in deposition process was recorded by In-situ Optical Microscopy.

Electrochemical measurements

CHI660E electrochemical workstation was used for cyclic voltammetry (CV), electrochemical impedance spectrum (EIS), linear sweep voltammetry (LSV), Tafel plots, and chronoamperometry (CA) tests. LSV curves and Tafel plots were measured using a three-electrode system that Zn plate as the working electrode, Pt plate as the counter electrode and Ag/AgCl as the reference electrode, respectively. The scanning voltage range for LSV curves was −1.5~−0.9 V, with a scan rate of 2 mV s^{-1}; the Tafel curve test was performed by scanning from −1.3 V to −0.7 V at a fixed rate of 1 mV s^{-1}. The CA measurements were examined on Zn||Zn symmetric cells by applying a constant potential of −150 mV. The frequency range for EIS tests was 0.01~10^5 Hz, with an amplitude of 5 mV. LAND CT3002A was employed for galvanostatic charge-discharge (GCD), rate performance tests, long cycle performance, and coulombic efficiency (CE) tests. Zn||Zn symmetric cells were assembled to test the cyclic performance at 1, 5, 10 mA cm^{-2} with the capacity of 1, 5, 10 mAh cm^{-2}. The rate performance of the Zn||Zn symmetric cells were tested at the current density of 0.1, 1, 2, 5, and 10 A g^{-1}. Zn||NVO full cells were assembled for CV measurements at a scan rate of 0.5 mV s^{-1} with the potential window of 0.2~1.6 V.

The electric double layer capacitance (EDLC) of Zn||Zn symmetric cells was analyzed by CV at different sweep rates, and the test voltage range was −15 mV to 15 mV. EDLC was calculated through the equation of $C= i/v$ (C, capacitance; i, current; v, scan rate). The value of i was obtained by taking half of the current difference between positive and negative scan under each scanning rate.

The transference number of Zn^{2+} was measured by Zn||Zn symmetric cell using Bruce-Vincent method. The i-t curves measured with a bias voltage of 10 mV, and the EIS plots were measured before and after polarization. The transference number of Zn^{2+} was calculated through the equation:

$$t_{Zn^{2+}} = \frac{I_s(V - I_0R_0)}{I_0(V - I_sR_s)}$$

V, the bias voltage (10 mV); I_0 and R_0 are the initial current and resistance; I_s and R_s are the steady state current and resistance.

Fabrication of cells

The Zn foil (diameter of 14 mm for Zn||Zn symmetric cells; 15 mm for Zn||Cu asymmetric cells and Zn||NVO full cells), Cu foil (diameter of 14 mm), NVO cathode (diameter of 14 mm) were used as electrodes. Glass fiber (diameter of 17 mm) was used as separator and 2 M $ZnSO_4$ with/without D-PA were used as electrolytes. All cells were assembled in CR2025-type coin cells containing 100 μL of electrolyte.

Theoretical calculations

The MD simulations were conducted using the Forcite module in Material Studio 2020, with the force field COMPASS II was selected for assigning charges. The solvent boxes were constructed using the Amorphous Cell, with periodic boundary conditions applied in the x, y,

and z directions. The system for simulating pure $ZnSO_4$ electrolyte contains 2778 water molecules, 100 Zn^{2+} and 100 SO_4^{2-}. The system for simulating $ZnSO_4$+D-PA electrolyte consists of 2220 water molecules, 100 Zn^{2+}, 100 SO_4^{2-}, and 58 D-PA molecules. First, the system was pre-equilibrated under the NVE ensemble at 298 K with a simulation time of 10 ps and a step size of 1 fs to ensure energy minimization. Subsequently, equilibrium was achieved using the Berendsen temperature control method under the NPT ensemble at 298 K, maintaining a 1 fs step size for 2 ns to ensure density convergence within a reasonable range. Finally, long-duration molecular dynamics simulations were performed under the NVT ensemble at 298 K with a 1 fs step size. The system was first equilibrated for 5 ns, followed by an additional 10 ns simulation to collect stable trajectories for statistical analysis. Based on the final trajectories to analyze radial distribution functions (RDFs, g(r)).

The adsorption energies of molecules on different Zn crystal planes and binding energies were calculated using the VASP software through Density Functional Theory (DFT). The calculations employed plane-wave pseudopotential techniques and the PBE (Perdew-Burke-Ernzerhof) functional from the Generalized Gradient Approximation (GGA) to simulate electron exchange correlation functions. The custom energy cutoff was 500 eV. A 15 Å vacuum layer was constructed to eliminate interactions between periodic structures.

The formula for calculating adsorption energy is as follows:

$$E_{abs} = E_{total} - E_{D-PA/H2O} - E_{Zn}$$

where E_{abs} is the adsorption energy, E_{total} is the total energy of the system, $E_{D\text{-}PA/H2O}$ is the molecular energy of D-PA/H_2O, E_{Zn} is the energy of the single Zn crystal plane.

The formula for calculating binding energy is as follows:

$$E_{binding} = E_{total} - E_a - E_b$$

where $E_{binding}$ is the binding energy, E_{total} is the total energy of the system, E_a and E_b represent the energies of individual components within the system.

The formula for calculating the discharge depth of Zn foil as a Zn metal anode is as follows:

$$\mathrm{DOD} = \frac{y}{0.585x} \times 100\%$$

where x (μm) is the thickness of the Zn foil, y (mAh cm^{-2}) is the areal capacity of the Zn anode used in electrochemical testing.

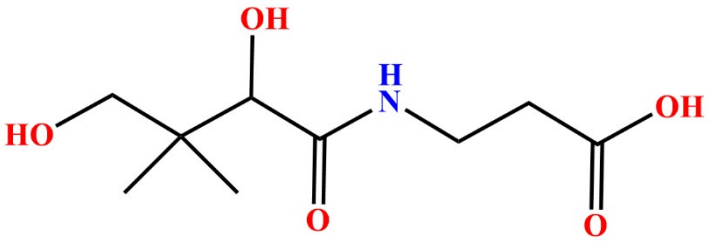

Figure S1. The chemical formula of D-Pantothenic Acid (D-PA).

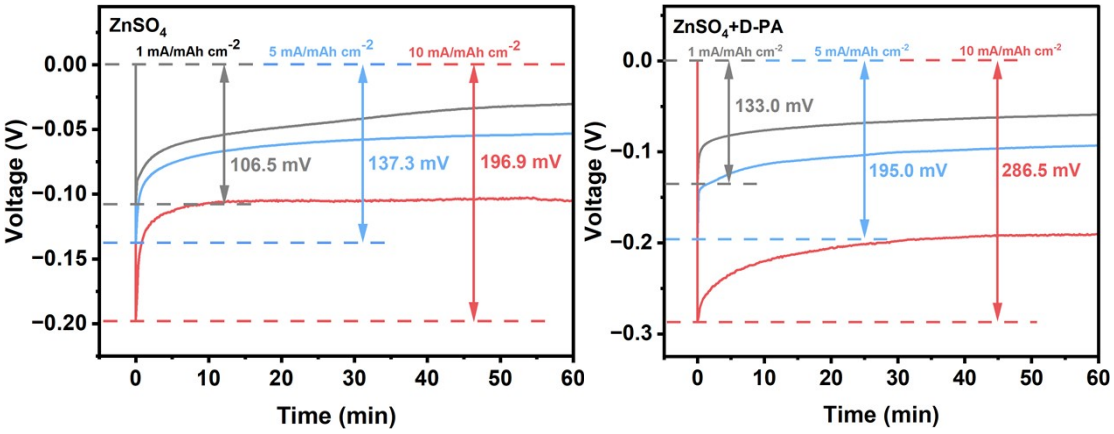

Figure S2. Comparison of nucleation overpotentials in $ZnSO_4$ electrolytes with/without D-PA via Zn||Zn symmetric batteries at different current densities (1, 5, 10 mA/mAh cm^{-2}).

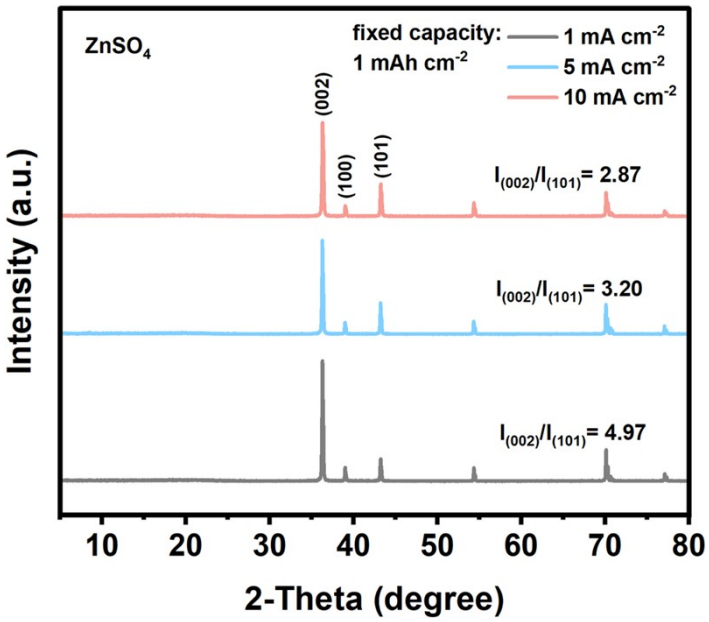

Figure S3. XRD pattern of pristine Zn foil cycled after 20 cycles at different current densities in $ZnSO_4$ electrolyte.

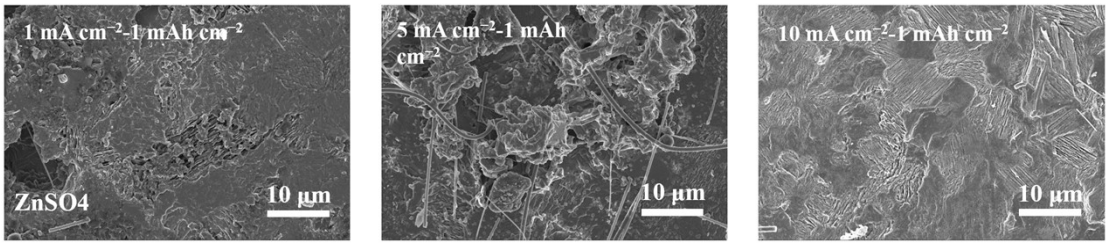

Figure S4. SEM images of Zn foil after 20 cycles in $ZnSO_4$ electrolyte at different current densities and fixed areal capacity.

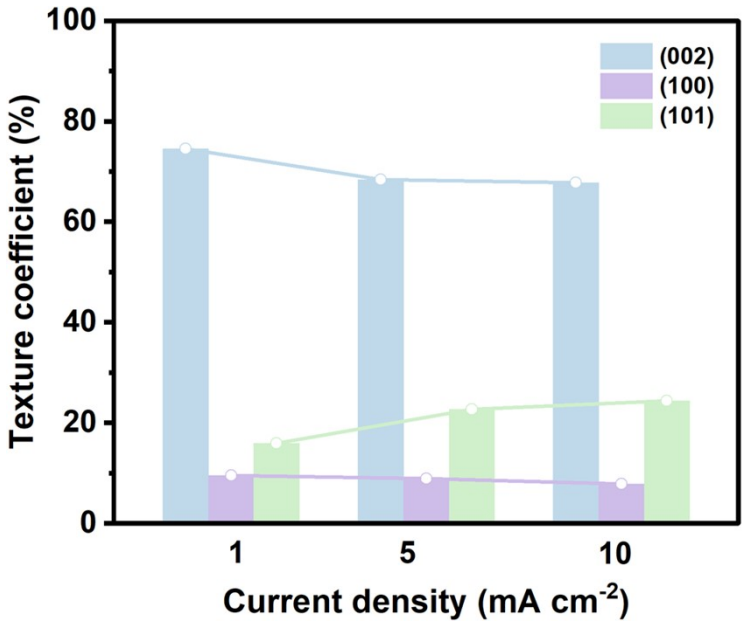

Figure S5. RTCs of different crystal planes of Zn products in $ZnSO_4$ electrolyte at different current densities.

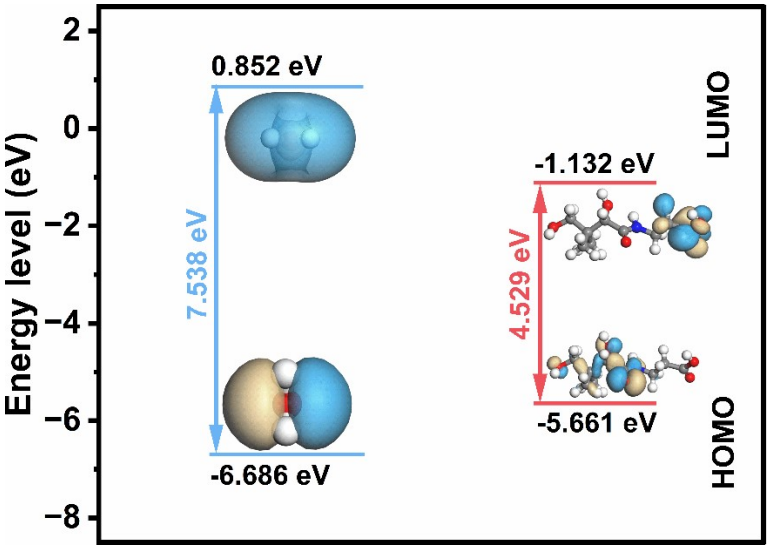

Figure S6. The HOMO and LUMO energy levels with corresponding iso-surfaces of H_2O and D-PA molecule.

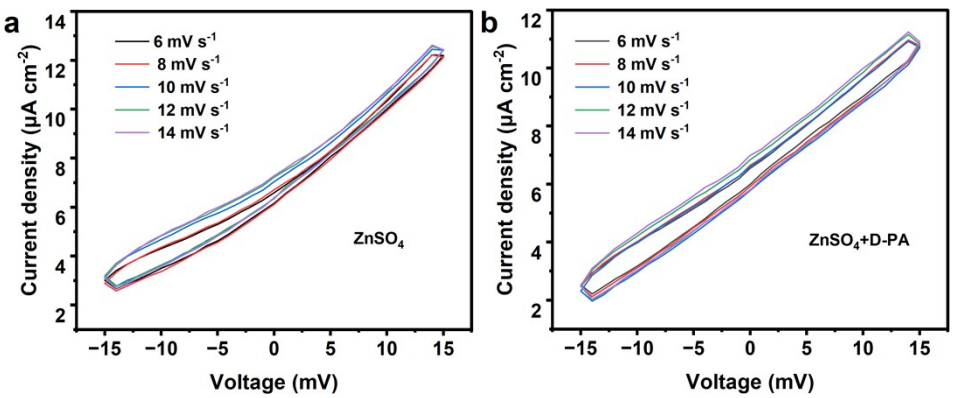

Figure S7. CV curves of Zn||Zn symmetrical cells in (a) $ZnSO_4$ and (b) $ZnSO_4$+D-PA electrolytes.

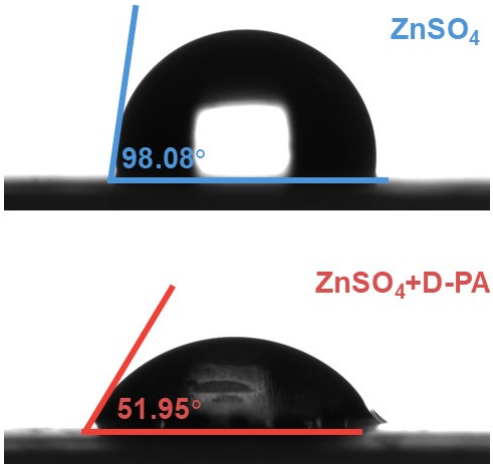

Figure S8. Contact angle of different electrolyte on Zn foil.

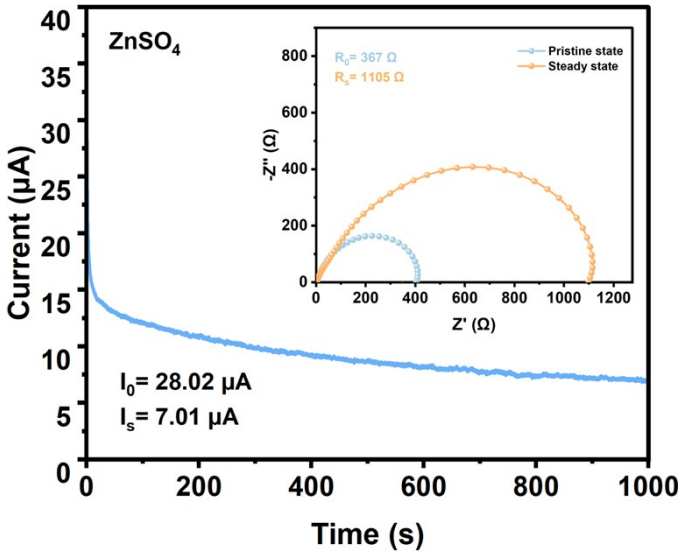

Figure S9. Current-time curve and EIS plots before and after polarization for the Zn||Zn cells in $ZnSO_4$ electrolyte.

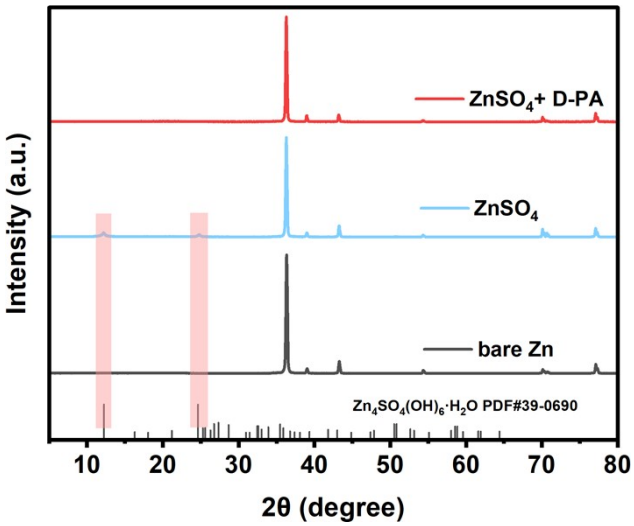

Figure S10. XRD spectra of immersion of Zn foil in $ZnSO_4$ electrolytes with/without D-PA for 7 days.

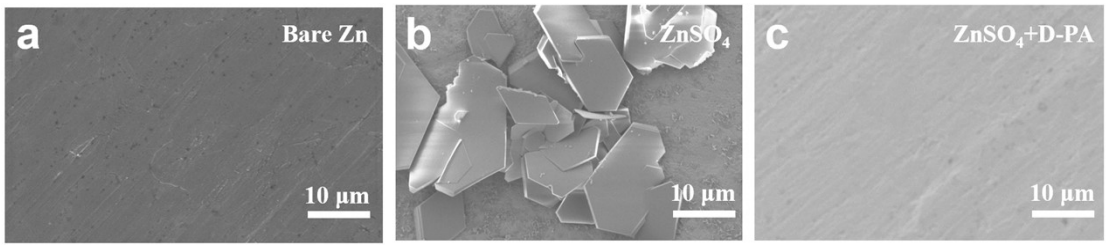

Figure S11. SEM images of immersion of Zn foil in $ZnSO_4$ electrolytes with/without D-PA for 7 days.

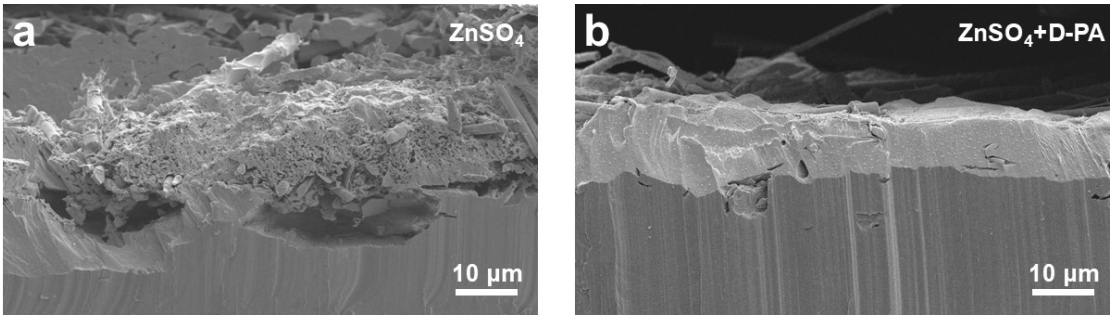

Figure S12. Cross-sectional SEM images of Zn anodes collected from Zn||Zn symmetric cells after 100 cycles at 10 mA/mAh cm^{-2} in (a) $ZnSO_4$ electrolyte and (b) $ZnSO_4$+D-PA electrolyte.

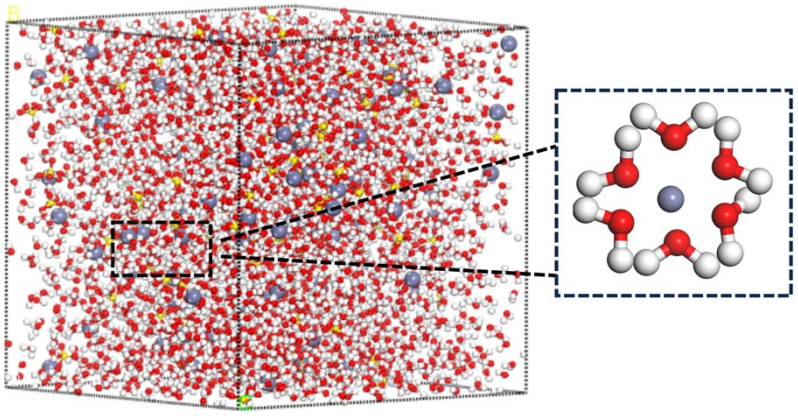

Figure S13. 3D snapshot of $ZnSO_4$ electrolyte obtained from MD simulations and the local solvation structure of hydrated Zn^{2+}.

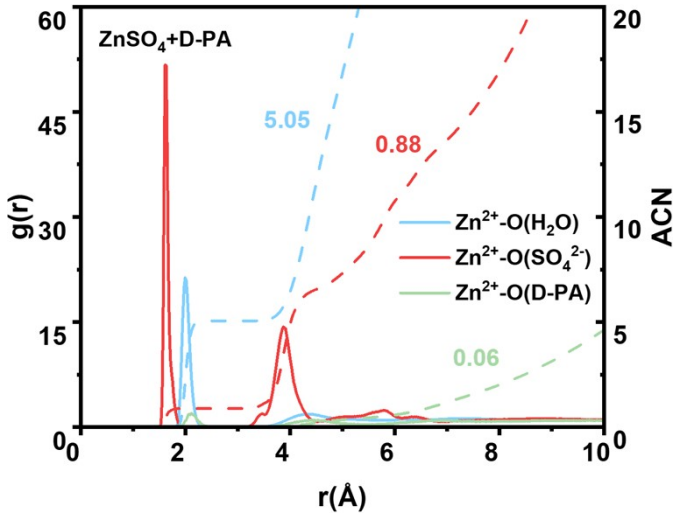

Figure S14. RDFs for Zn^{2+}-O(H_2O), Zn^{2+}-O(D-PA) and Zn^{2+}-O(SO_4^{2-}) from MD simulations in $ZnSO_4$+D-PA electrolytes.

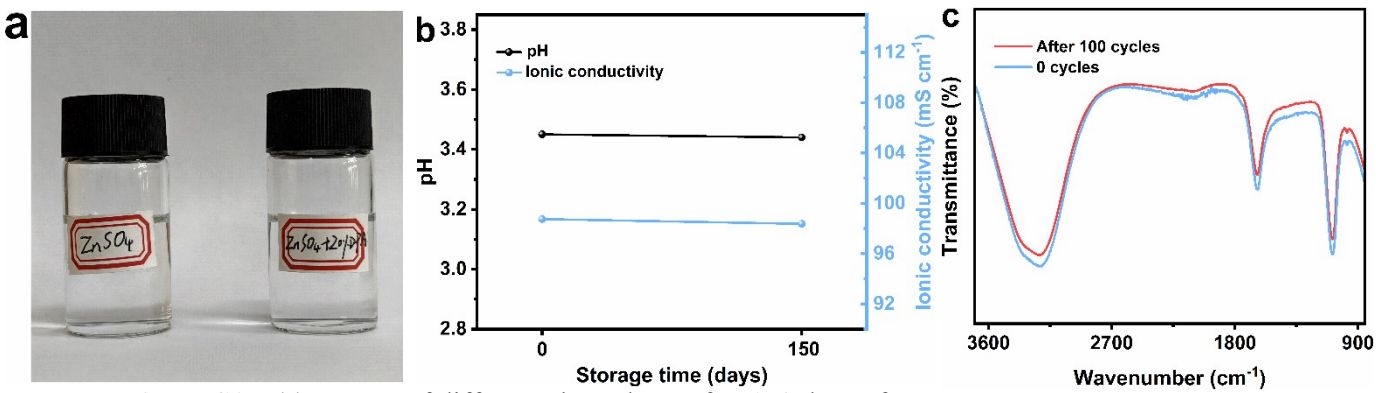

Figure S15. (a) Images of different electrolytes after 150 days of storage at room temperature. (b) $ZnSO_4$+D-PA electrolyte pH and conductivity curves after 150 days of storage at room temperature. (c) FTIR spectra of $ZnSO_4$+D-PA electrolyte before and after 100 cycles.

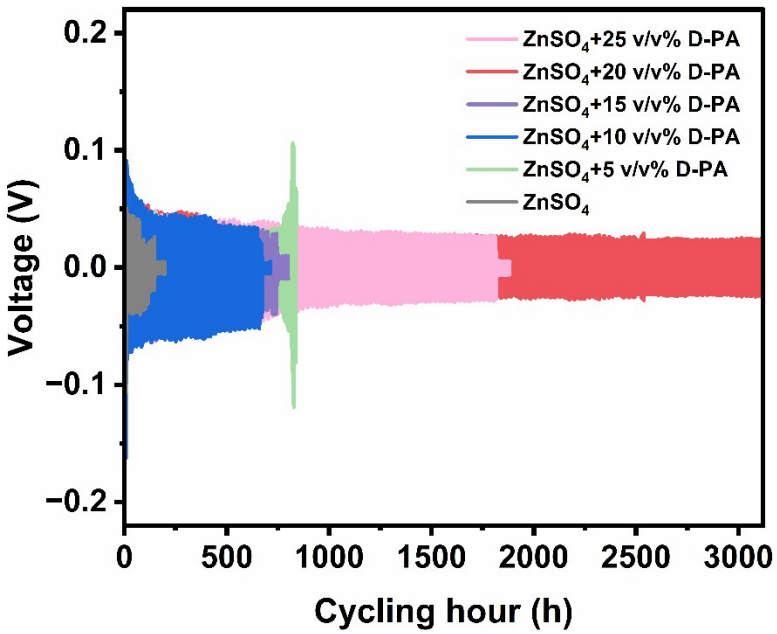

Figure S16. Cyclic performance of Zn||Zn symmetric cell in different electrolytes at the current density of 1 mA cm^{-2} and capacity of 1 mAh cm^{-2}.

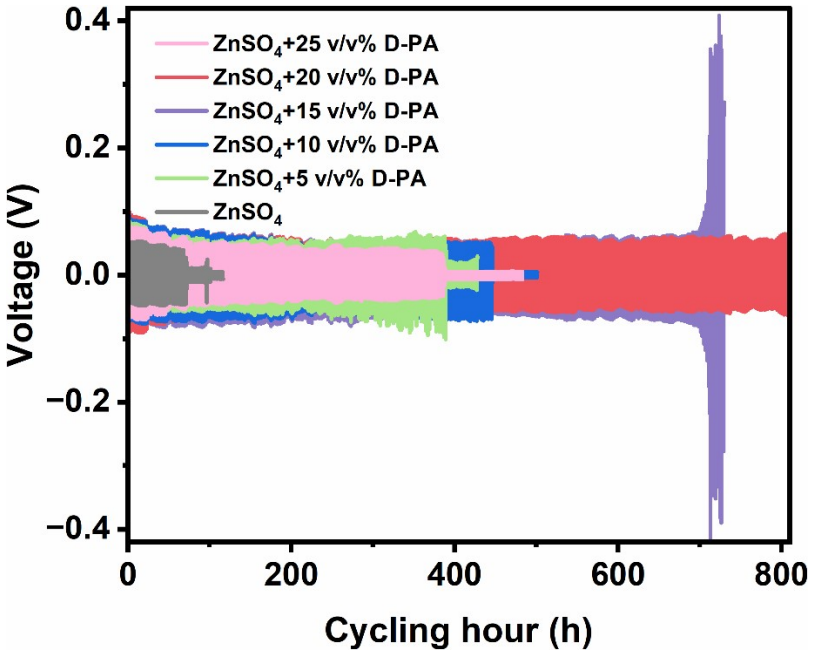

Figure S17. Cyclic performance of Zn||Zn symmetric cell in different electrolytes at the current density of 5 mA cm^{-2} and capacity of 5 mAh cm^{-2}.

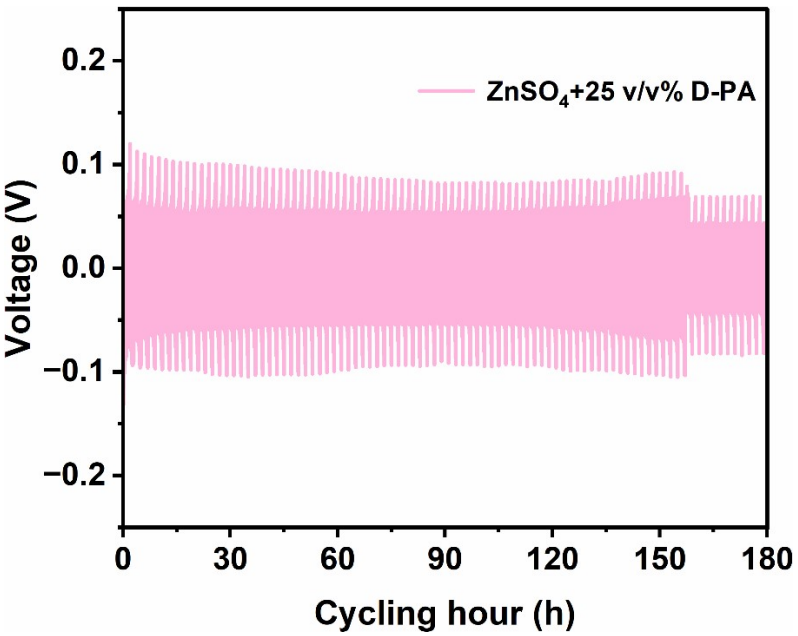

Figure S18. Cyclic performance of Zn||Zn symmetric cell in $ZnSO_4$+25 v/v% D-PA electrolyte at the current density of 10 mA cm^{-2} and capacity of 10 mAh cm^{-2}.

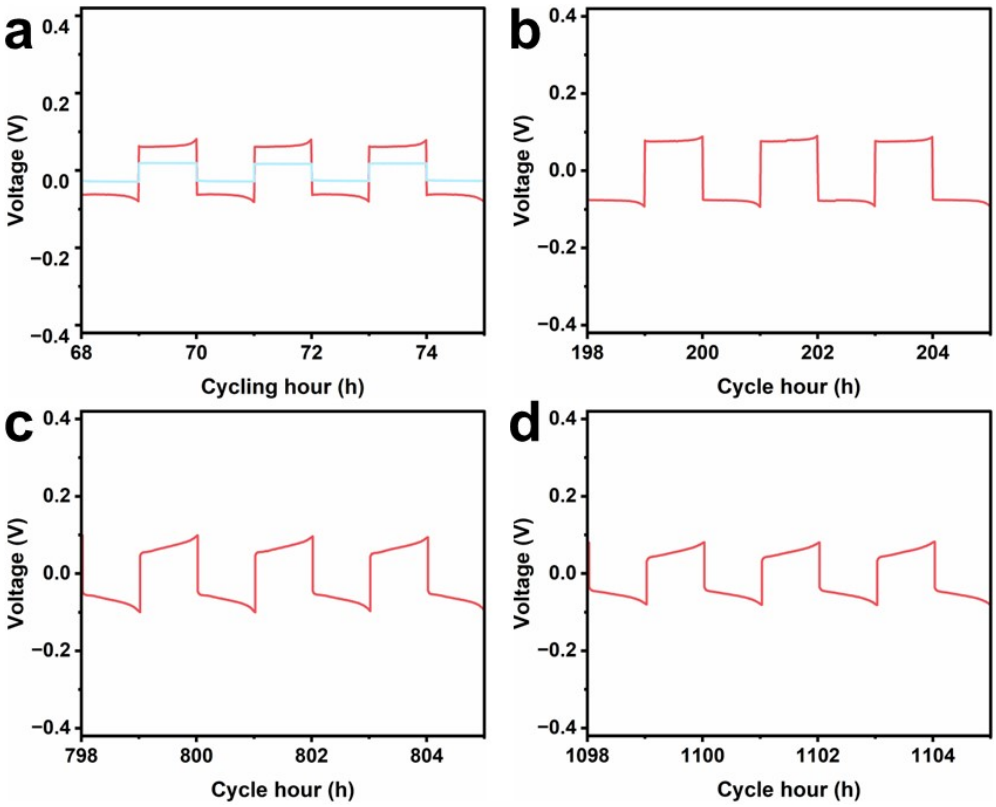

Figure S19. Amplified voltage curves at 10 mA cm^{-2} and 10 mAh cm^{-2}.

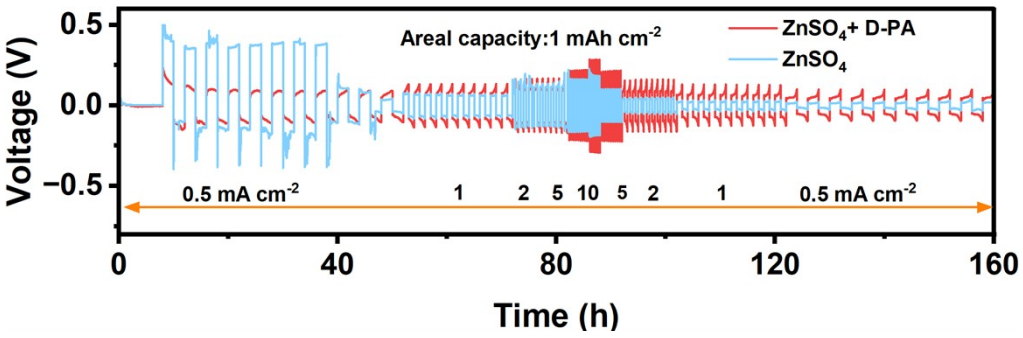

Figure S20. Rate capability of Zn||Zn symmetric cell at varied current density.

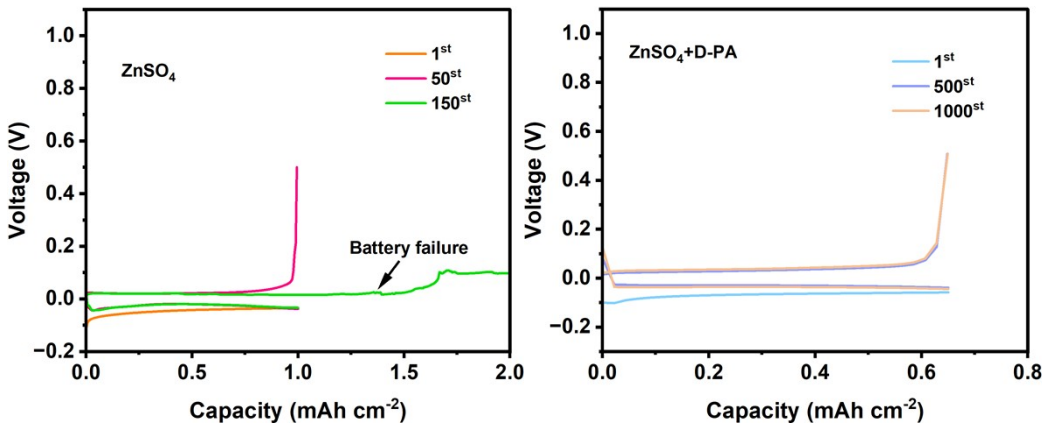

Figure S21. The corresponding voltage profiles of Zn||Cu cells in (a) $ZnSO_4$ and (b) $ZnSO_4$+D-PA electrolytes.

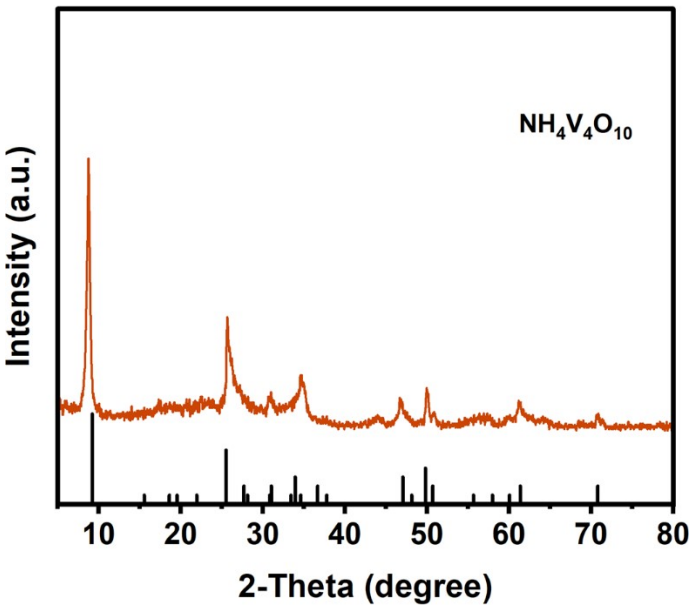

Figure S22. XRD pattern of NVO.

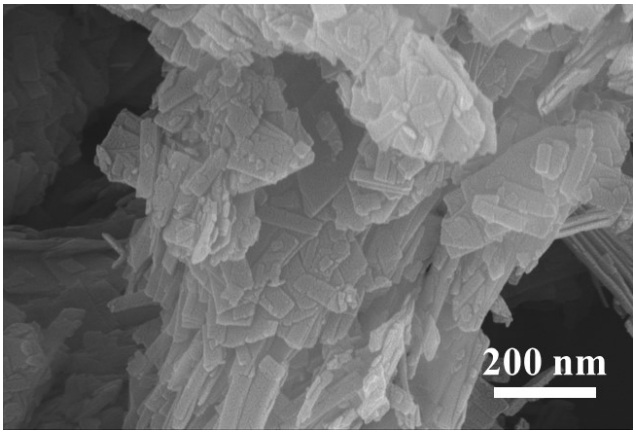

Figure S23. SEM image of NVO.

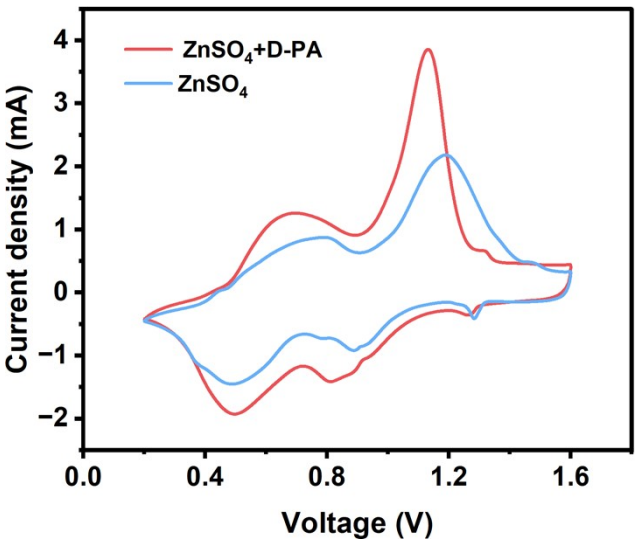

Figure S24. CV curves of the Zn||NVO full cells in different electrolytes at a scanning rate of 0.5 mV s^{-1}.

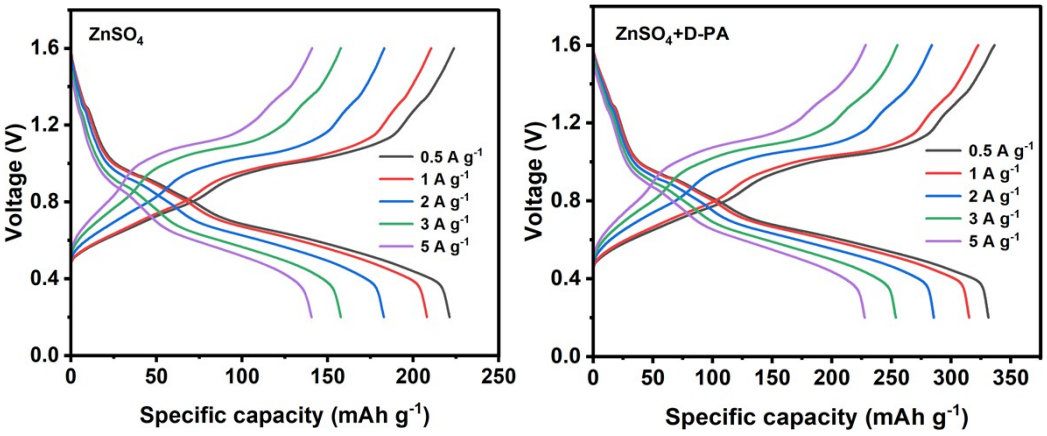

Figure S25. Charge-discharge profiles of Zn||NVO full cells at various current densities from 0.5 to 5.0 A g^{-1} in (a) $ZnSO_4$ and (b) $ZnSO_4$+D-PA electrolytes.

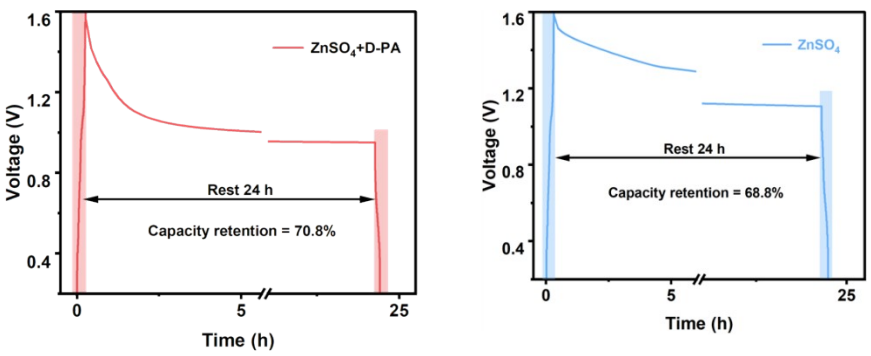

Figure S26. The capacity retention of Zn||NVO full cells in (a) $ZnSO_4$ and (b) $ZnSO_4$+D-PA electrolytes after charging at 1.6 V, resting for 24 h, and discharging to 0.2 V.

Table S1. Performance comparison of Zn symmetric cells in $ZnSO_4$ electrolytes with D-PA (D-pantothenic acid) and other reported electrolyte additives.

Electrolyte additive	Current density (mA cm^{-2})	Areal capacity (mAh cm^{-2})	Cycle time (hour)	Ref.
D-Pantothenic acid	10	10	1260	This work
MAAC	10	10	55	1
Butyrolactam	20	1	190	2
Vitamin C	10	10	300	3
$InCl_3$/ chitosan	5	5	350	4
Pyridine oxide	10	10	108	5
Xylenol Orange Tetrasodium Salt	5	5	1000	6
3-cyclobutene sulfone	5	5	400	7
Vitamin C	20	5	760	8
Disodium malate	5	5	750	9
Phenylalanine	8	8	610	10

References

1. Y. Luo, J. Yin, P. Chen, B. Wang, J. Xu, Z. Wang and K. Guo, *Small*, 2024, 20, 2310824.

2. Q. Guo, G. Teri, W. Mo, J. Huang, F. Liu, M. Ye and D. Fu, *Energy Environ. Sci.*, 2024, 17, 2888-2896.

3. Z. Zhang, P. Wang, C. Wei, J. Feng, S. Xiong and B. Xi, *Angew. Chem. Int. Ed.*, 2024, 63, e202402069.

4. J. Song, Z. Ren, Z. Chen, S. Zhang, Z. Yu, J. Cheng and B. Wang, *Energy Storage Mater.*, 2025, 81, 104523.

5. Z. Li, Z. Wang, W. Sun, Y. Ma, W. Guo and Y. Fu, *Adv. Mater.*, 2025, 37, 2420489.

6. C. Wang, D. Zhang, Y. Shi, C. Tan, Y. Yang, R. Zhang, J. Xie, G. Sun, H. Qiu, M. Cao, Y. Ji and L. Li, *Adv. Funct. Mater.*, 2025, 35, 2508251.

7. H. Cui, W. Li, H. Chen, Z. Liu and D. Zhou, *J. Energy Chem.*, 2025, 109, 455-465.

8. J. Zhang, Q. Wu, S. Yang, F. Luo, Y. Li, Y. Zhang, K. Chen, J. Huang, H. Xie and Y. Chen, *Green Chem.*, 2024, 26, 6723-6734.

9. H. Ji, Y. Liang, T. Yang, H. Wu, O. Sheng, T. Shen, C. Dong, T. Du, L. Yin, J. Zhang, R. Zheng and X. Zhang, *J. Mater. Sci. Technol.*, 2026, 240, 56-64.

10. C. Ping, X. Yu, S. Huang, Y. Zhou, L. Song, L. Chen, M. Wang and Y. Zhang, *J. Energy Storage*, 2026, 141, 119198.